fibers

MDPI

Article

Experimental Study on Strength Development, Water Absorption and Microstructure of Naturally Aged Hybrid Glass Fiber and Polypropylene Fiber-Reinforced Concrete

Lihui Yin and Zhu Yuan *

School of Civil Engineering, Heilongjiang University, Harbin 150080, China
* Correspondence: 2025105@hlju.edu.cn

Abstract

This paper presents a systematic investigation into the long-term mechanical property development, water absorption behavior, and microstructural characteristics of hybrid glass and polypropylene fiber-reinforced concrete (HGPFRC). The findings provided valuable engineering construction solutions for holistically considering the improvement effect of hybrid fibers on concrete performance and for the durability design of concrete materials. The main conclusions of the study are as follows: the water-to-binder ratio (w/b) and the hybrid fiber content significantly influenced the development rate of compressive strength in concrete. Compared to the control group without fibers, the compressive strength of HGPFRC increased more rapidly during the curing stage from 7 to 28 days. HGPFRC with different w/b and fiber contents exhibited significant differences in water absorption rates at various testing stages. In this study, the water absorption of HGPFRC reached 60% to 86% of the total absorption on the first day, 6% to 23% from the second to the fourth day, and 3% to 18% from the fifth to the thirty-first day. Considering the compressive strength, water absorption performance, and microstructure observed via SEM, the optimal mix proportion for the HGPFRC in this study was determined to be a w/b of 0.35 and a hybrid fiber content of 1.8%. The hybrid glass and polypropylene fiber content of 2.7% used in this study exceeded the optimal dosage, and the resulting concrete could not meet engineering construction requirements.

Keywords: fiber-reinforced concrete; hybrid fibers; long-term strength development; water absorption properties; microstructure

Check for updates

Academic Editor: Francesco Bencardino

Received: 10 March 2026
Revised: 22 March 2026
Accepted: 25 March 2026
Published: 26 March 2026

Copyright: © 2026 by the authors. Licensee MDPI, Basel, Switzerland. This article is an open access article distributed under the terms and conditions of the Creative Commons Attribution (CC BY) license.

1. Introduction

Concrete is one of the most widely used construction material worldwide. However, due to numerous inherent limitations such as low tensile strength, poor ductility, high brittleness, and poor impact resistance, it faces significant constraints in engineering applications [1–5]. Incorporating discontinuous chopped fibers is one method to enhance concrete properties. The characteristics of fiber-reinforced concrete (FRC) depend on the type, quantity, and size of the added fibers. Commercially available fibers encompass a wide variety, including steel fibers, glass fibers, synthetic fibers, and certain natural fibers [6–24]. Among these, glass fibers (GF) and polypropylene fibers (PPF) offer significant cost advantages during construction projects due to their lower prices. Consequently, as the two micro-reinforcing materials currently used to enhance concrete performance, they possess the fundamental conditions for widespread application in engineering construction.

Research findings have been published regarding the performance enhancement effects of GF or PPF on concrete. Adding GF could significantly improve the mechanical properties of mortar and concrete, enhancing compressive, flexural, and tensile strengths [25–29]. Low-dose GF could effectively control early cracking in ordinary and self-compacting concrete by reducing the area and maximum length of concrete cracks [30]. However, due to the inherent brittleness of GF, their effectiveness in improving concrete brittleness was far inferior to that of steel fibers or polymer fibers [26,28]. Partially replacing ordinary Portland cement with mineral admixtures (e.g., silica fume) yielded synergistic benefits beyond the sum of individual additions. Silica fume-reduced water absorption and chloride permeability in FRC while enhancing acid resistance [31].

PPF exhibited low elastic modulus, high strength, and excellent ductility. PPF effectively suppressed cracks in cementitious matrix during both the initial cracking stage and crack propagation phase. They enhanced load-bearing capacity after peak loading, enabling a failure mode characterized by "cracking without breaking" [32,33]. However, conflicting conclusions existed regarding the improvement of concrete compressive strength by PPF [26,34–38].

Incorporating a single type of fiber was only effective within the limited strain range and crack opening range of the cementitious matrix. Therefore, it could only enhance specific properties of the composite material, such as strength or ductility. Fiber hybridization provided an effective approach for comprehensively improving concrete performance. Simultaneously incorporating high-modulus and high-ductility fibers into the cement matrix enabled both fiber types to enhance strength and toughness at different loading stages and structural levels within the cementitious matrix, thereby improving numerous engineering properties of the composite material [39,40]. For instance, this approach enhanced compressive and flexural strength, significantly increased chloride-ion permeability resistance, and positively influenced concrete ductility [41,42]. It altered the failure mode of concrete, prolonged the descending segment of the stress–strain curve [43], enhanced fracture toughness [44], effectively refined large pore sizes and reduced porosity [45], significantly improved freeze–thaw resistance, and markedly extended the service life of structures in cold regions [46].

Given the relatively low cost of both GF and PPF, along with the characteristics of these two fiber materials, incorporating a hybrid of these fibers into concrete to produce HGPFRC may offer an excellent solution for comprehensively addressing both high-performance concrete requirements and construction cost considerations [5,47,48].

Currently, several critical gaps remain in the research on HGPFRC that warrant further investigation. First, the combined effects of high fiber volume fractions (e.g., up to 2.7%) and a wider range of w/b (e.g., from 0.30 to 0.40) remain underexplored. Both the mechanical properties and durability of HGPFRC critically depend on fiber content and w/b. Existing studies have typically confined fiber content to relatively low percentages or limited w/b to narrow ranges, leaving the interactive effects under conditions of high fiber dosage and varying cementitious matrix densities largely unclear. Second, and most importantly, the vast majority of current research has focused on short-term performance, usually only considering curing ages of 7 and 28 days. The ultra-long-term performance of HGPFRC, particularly its behavior after several years, has been largely overlooked. Understanding the evolution of mechanical properties and microstructure over extended periods (e.g., 3 years) is essential for predicting the long-term durability and service life of structures. Furthermore, water absorption is a key indicator of concrete durability, yet, the evolution of water absorption properties of HGPFRC over time requires systematic investigation.

This study aims to address the aforementioned gaps, with its scientific contributions being: (1) systematically revealing the interactive effects between a high range of hybrid

fiber volume fractions (0.9–2.7%) and a wide range of w/b (0.30–0.40), thereby identifying the optimal fiber content intervals for different cementitious matrix densities; (2) reporting, for the first time, the compressive strength evolution and microstructural characteristics of HGPFRC at an ultra-long age of 3 years; (3) establishing a correlation analysis between the 3-year microstructural characteristics and macroscopic water absorption properties, providing an experimental basis for the long-term durability design of HGPFRC.

2. Experimental Procedure

2.1. Raw Materials and Mix Proportions

The cement used was P•O42.5 ordinary Portland cement. Mineral admixtures included fly ash, silica fume, and ground granulated blast furnace slag. The chemical compositions of the cement and mineral admixtures are shown in Table 1. The fine aggregate was high-quality natural river sand, and the coarse aggregate was graded crushed stone with a particle size range of 5–20 mm. The water reducer used was a polycarboxylic water-reducing agent. The fibers used were short cut GF and PPF with a length of 12 mm. The appearance of the fibers is shown in Figure 1, and the performance parameters, as provided by the manufacturer (Ningxiang Building Materials Co., Ltd., Changsha, China), are shown in Table 2.

Table 1. Chemical compositions of cement and mineral admixtures.

Chemical Compositions (%)	Cement	Fly Ash	Silica Fume	Slag
SiO_2	21.50	66.67	93.82	32.08
CaO	59.81	3.05	0.41	38.09
Al_2O_3	5.86	18.97	0.21	15.06
Fe_2O_3	2.85	4.39	0.00	0.94
MgO	2.23	1.24	0.65	8.26
SO_3	2.06	0.30	0.64	0.17
Na_2O	0.20	-	0.32	-
K_2O	0.67	-	0.85	-
Loss on ignition	4.82	5.38	3.10	5.40



(**a**) (**b**)

Figure 1. The appearance of the fibers: (**a**) GF and (**b**) PPF.

The concrete mix design was conducted in accordance with standard JGJ 55-2011 [49]. Three water/binder ratios were set: 0.30, 0.35, and 0.40. The selection of fiber volume fractions was based on the following considerations: (1) a review of the literature indicated that the total fiber content in HGPFRC typically did not exceed 1% [42,50]; (2) preliminary

experiments by the authors showed that total fiber content exceeding 2.7% led to a significant decline in the workability of the concrete mixture, making adequate compaction difficult; and (3) this study aimed to systematically investigate the effects across a broad spectrum of fiber contents, from conventional (0.9%) to high (2.7%), to identify the optimal hybrid fiber content and the potential onset of negative hybrid effects. Accordingly, three fiber volume fractions were selected: 0.9% (low), 1.8% (medium), and 2.7% (high). In all hybrid mixtures, glass and polypropylene fibers were incorporated at equal volume fractions. A control group with zero fiber content was also included in the experimental program. The mix proportions for HGPFRC are detailed in Table 3. In the mix ID, such as "HF-0.30-1.8", the "HF" means hybrid fibers, the "0.30" means a w/b of 0.30, and the "1.8" means a total hybrid fiber volume fraction of 1.8%. Additionally, the "HF-0.30-0" was denoted the control group without fiber addition at a w/b of 0.30.

Table 2. Physical and mechanical parameters of GF and PPF.

Type of Fiber	Length (mm)	Diameter (μm)	Aspect Ratio	Specific Gravity (g/cm^3)	Tensile Strength (MPa)	Elastic Modulus (MPa)
GF	12	15	800	2.36	1500	4286
PPF	12	60	200	0.91	486	4800

Table 3. The mix proportions of the HGPFRC.

Mix ID	Water/ Binder Ratio	Cement (kg/m^3)	Fly Ash (kg/m^3)	Silica Fume (kg/m^3)	Slag Powder (kg/m^3)	Fine Aggregate (kg/m^3)	Coarse Aggregate (kg/m^3)	Water (kg/m^3)	Water Reducer (kg/m^3)	Volume Fraction of Fiber (%)	
										GF	PPF
HF-0.30-0	0.30	280	86	22	43	655	1165	129	6.45	-	-
HF-0.30-0.9	0.30	280	86	22	43	655	1165	129	6.45	0.45	0.45
HF-0.30-1.8	0.30	280	86	22	43	655	1165	129	6.45	0.90	0.90
HF-0.30-2.7	0.30	280	86	22	43	655	1165	129	6.45	1.35	1.35
HF-0.35-0	0.35	240	74	18	37	677	1204	129	5.55	-	-
HF-0.35-0.9	0.35	240	74	18	37	677	1204	129	5.55	0.45	0.45
HF-0.35-1.8	0.35	240	74	18	37	677	1204	129	5.55	0.90	0.90
HF-0.35-2.7	0.35	240	74	18	37	677	1204	129	5.55	1.35	1.35
HF-0.40-0	0.40	210	65	16	32	694	1234	129	4.85	-	-
HF-0.40-0.9	0.40	210	65	16	32	694	1234	129	4.85	0.45	0.45
HF-0.40-1.8	0.40	210	65	16	32	694	1234	129	4.85	0.90	0.90
HF-0.40-2.7	0.40	210	65	16	32	694	1234	129	4.85	1.35	1.35

2.2. Specimen Preparation and Curing

Concrete specimens were prepared as cubes with dimensions of 100 × 100 × 100 mm^3, totaling 216 specimens. The preparation process of the specimens was carried out in accordance with the specifications CECS13-2009 [51] and GB/T 50081-2019 [52]. The raw materials were mixed using a forced mixer. The sequence of raw material addition and the mixing duration were as follows: coarse aggregate, fine aggregate, cement, fly ash, silica fume, and slag powder were first placed into the mixer and dry-mixed for 40 s. Subsequently, 30% of the water was added and mixed for 90 s. The fibers, along with another 30% of the water, were then introduced and mixed for an additional 90 s. Finally, the superplasticizer and the remaining water were added, and mixing continued until the mixture transformed from a granular state into a cohesive colloidal consistency. The fresh concrete was placed into molds and compacted using a vibrating table. After casting, the specimens were stored in the laboratory for 24 h prior to demolding. The curing regime was as follows: specimens were first cured in water under standard conditions for 28 days.

After this initial curing period, the specimens designated for continued aging were stored in the laboratory until the age of 3 years, under controlled conditions at a temperature of 24 ± 2 °C and a relative humidity of 40 ± 3%.

3. Test Procedures

3.1. Compressive Strength Test

A total of 108 cube specimens were used to test the compressive strength of concrete at 7 d, 28 d, and 3 years. Testing was conducted in accordance with standard GB/T 50081-2019 [52]. A YAW-2000A microcomputer-controlled electro-hydraulic servo universal testing machine was employed. Compressive strength values were calculated according to specifications CECS13:2009 [51] and GB/T 50081-2019 [52]. In the test, three specimens were tested per group, and the average value of the test data was taken as the strength value to minimize errors.

3.2. Full Curve Test of Water Absorption

A total of 72 cubic specimens were used to test the water absorption properties of the concrete. The water absorption test was conducted according to ASTM C642-2013 [53]. The specimens were dried in a 60 °C oven for 7 days, weighed using an electronic scale, and their initial weights recorded. The testing was conducted using a fully immersed water absorption test. During the initial 4 days of the test, concrete specimens were weighed daily. After 4 days, as the water absorption rate decreased, weighing was conducted every 3 days until the 37th day. Three specimens were tested per group, and the average of the test values was taken as the test result.

3.3. SEM Testing

The microstructure observation test procedure was conducted in accordance with ASTM C1723-2010 [54]. A Thermo Scientific, Waltham, MA, USA, Apreo S HiVac scanning electron microscope was used to examine the microstructure of concrete at 3 ages. Figure 2 shows a portion of concrete specimens placed on the scanning stage of the Apreo, Menlo Park, CA, USA, SEM after surface gold-sputtering treatment.

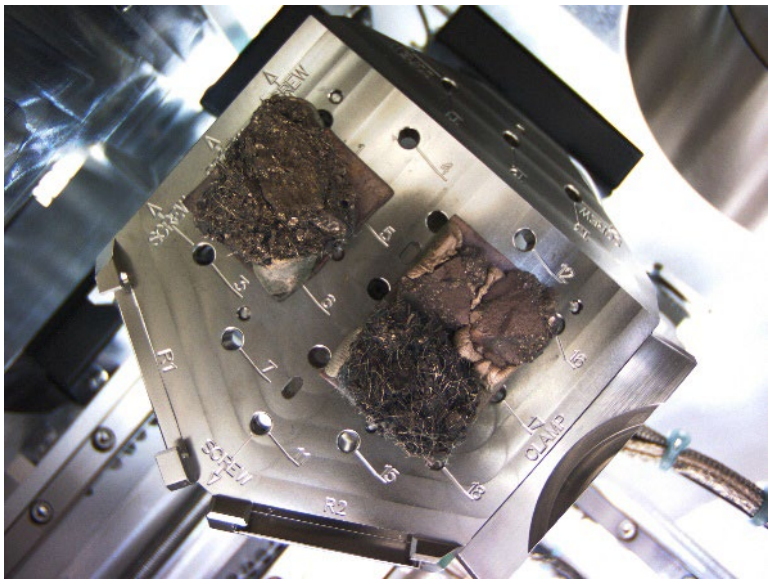


Figure 2. A tiny portion of specimens placed on the Apreo SEM scanning workbench.

4. Results and Discussion

4.1. Compressive Strength

Figure 3 shows the compressive strength of HGPFRC. The w/b and the dosage of hybrid fibers exert varying degrees of influence on the compressive strength of concrete at different curing ages.

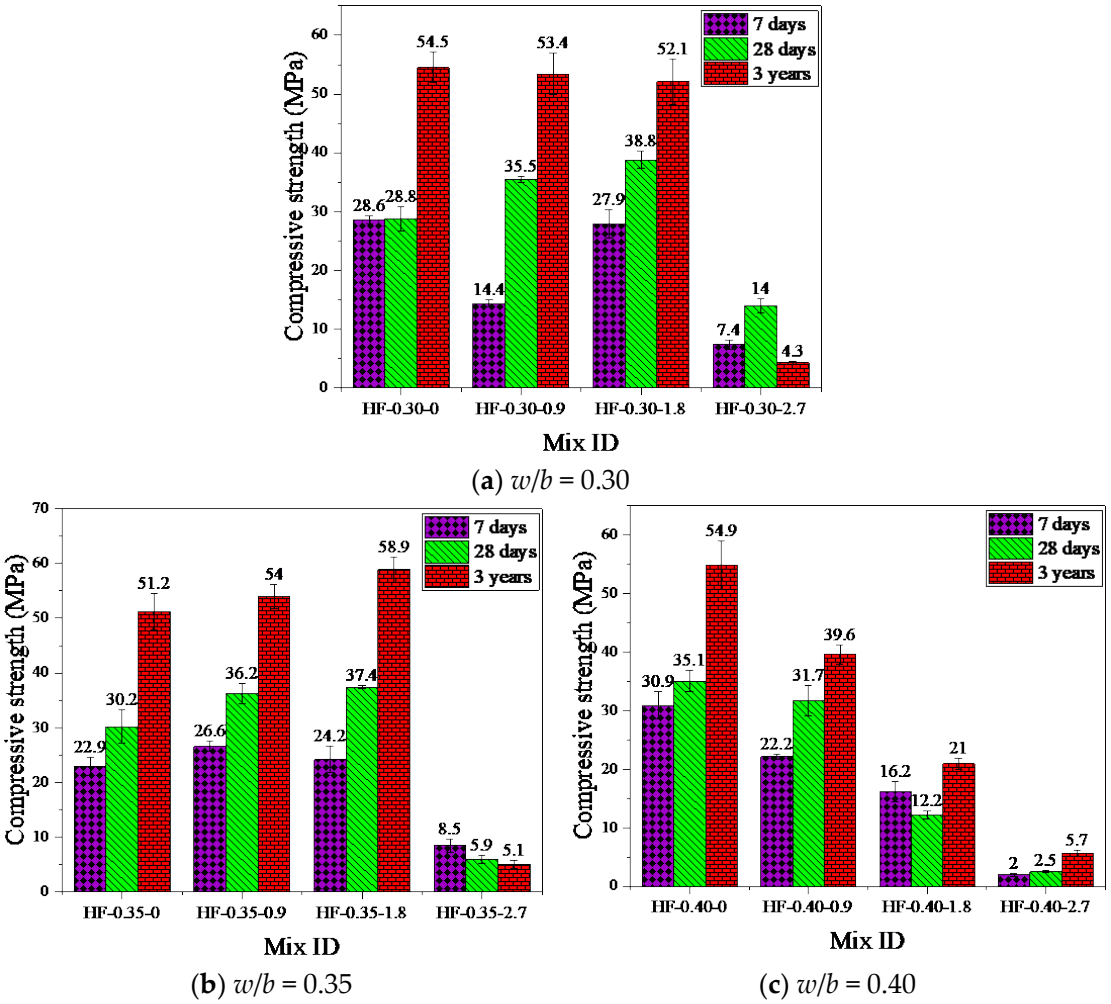


Figure 3. The compressive strengths of HGPFRC.

For the 7-day compressive strength of HGPFRC, it can be observed that when w/b = 0.30, the 7-day compressive strength of HF-0.30-0.9 was only 14.4 MPa, based on empirical analysis, this value was considered excessively low and was therefore treated as an outlier. Overall, the 7-day compressive strengths of all HGPFRC specimens were lower than that of the fiber-free control group, HF-0.30-0, which was 28.6 MPa. At a w/b of 0.35, the control group HF-0.35-0 exhibited a strength of only 22.9 MPa. For the HGPFRC specimens, cpressive strength gradually decreased as the fiber content increased. Specifically, the 7-day compressive strengths of HF-0.35-0.9 and HF-0.35-1.8 were 26.6 MPa and 24.2 MPa, respectively. When w/b = 0.40, all HGPFRC specimens exhibited lower 7-day compressive strengths than HF-0.40-0, with strength decreasing as fiber content increased. At a fiber dosage of 2.7%, the compressive strength of HF-0.40-2.7 plummeted to 2 MPa, representing a 93.5% reduction compared to HF-0.40-0.

For the 28-day compressive strength of HGPFRC, it is observed that when w/b = 0.30 and 0.35, the compressive strength exhibited the same trend with increasing fiber dosage: first increasing and then sharply decreasing. The addition of 0.9% and 1.8% hybrid

fibers significantly enhanced compressive strength, with 1.8% being the optimal content. At this point, the compressive strength increased to 38.8 MPa and 37.4 MPa respectively, representing increases of 34.7% and 23.8% compared to HF-0.30-0 and HF-0.35-0. When w/b = 0.40, incorporating hybrid fibers reduced compressive strength, with strength values decreasing as fiber content increased. The 28-day compressive strength of HF-0.40-2.7 was only 2.5 MPa. This finding suggests that when the fiber dosage exceeds a certain threshold, the reinforcing effect of the fibers can be offset—or even reversed into a significant negative effect—by defects in the cementitious matrix, particularly in the absence of a sufficiently low w/b.

For the 3-year compressive strength of HGPFRC, at a w/b of 0.30, considering the margin of error, the 3-year compressive strengths of HF-0.30-0, HF-0.30-0.9, and HF-0.30-1.8 were essentially comparable. At a w/b of 0.35, it can be observed that as the fiber content increased, the compressive strengths of HF-0.35-0.9 and HF-0.35-1.8 increased from 51.2 MPa (for HF-0.35-0) to 54 MPa and 58.9 MPa, respectively. A fiber content of 1.8% was identified as the optimal dosage for HGPFRC at a w/b of 0.35 at the age of 3 years. At a w/b of 0.40, the 3-year compressive strengths of HF-0.40-0.9 and HF-0.40-1.8 decreased sharply to 39.6 MPa and 21 MPa, respectively, compared to 54.9 MPa for the control group HF-0.40-0.

GF and PPF, when added at appropriate proportions, were uniformly distributed throughout the cement mortar matrix. They complemented each other and worked synergistically to provide reinforcement at different structural levels, delivering their combined effects throughout all stages of loading [55]. GF possessed significantly higher strength and elastic modulus than the cement matrix, enhancing concrete at the macroscopic level. When macroscopic cracks developed in the GF-reinforced matrix, these cracks propagated across the cross-section. Upon reaching elevated stress levels, the fibers' load-bearing capacity rapidly diminished as deformation increased [56]. PPF possessed stiffness comparable to the matrix. Before initial crack initiation, their effect was negligible and did not significantly enhance the concrete's initial crack strength. However, PPF exhibited excellent ductility with large fracture strain. Thus, PPF toughened the composite material at a more microscopic level. Moreover, due to their low elastic modulus, PPF exhibit tensile failure or tensile-pullout failure within the composite. Consequently, crack propagation was impeded or halted by the PPF, thereby increasing the average fracture strain of the GF and enabling HGPFRC to exhibit a composite failure mechanism [44,57].

Figure 4 illustrates the compressive strength increase of HGPFRC at different curing ages. In the figure, the "$I_{28d\text{-}7d}$" was denoted as the increase percentage in HGPFRC's 28-day compressive strength relative to its 7-day value, and the "$I_{3y\text{-}28d}$" represented the increase percentage in the 3-year compressive strength compared to the 28-day value. Typically, both $I_{28d\text{-}7d}$ and $I_{3y\text{-}28d}$ are positive values. The negative values observed in Figure 4 could be attributed to the following reason: As the w/b and fiber dosage increased, the amount of cementitious material available to encapsulate fibers within the concrete became insufficient. This led to uneven mixing during specimen preparation, causing fiber "clumping". Consequently, weak points within the concrete structure were introduced.

At different w/b, the $I_{28d\text{-}7d}$ of the control group was lower than that of HGPFRC, while the $I_{3y\text{-}28d}$ of the control group was higher than that of HGPFRC, except for HF-0.40-1.8 and HF-0.40-2.7. That is, compared to the control group concrete, HGPFRC exhibited faster compressive strength development between days 7 and 28. During the first 7 days of curing, as well as from day 28 to 3 years, the strength of control group developed more rapidly than HGPFRC.

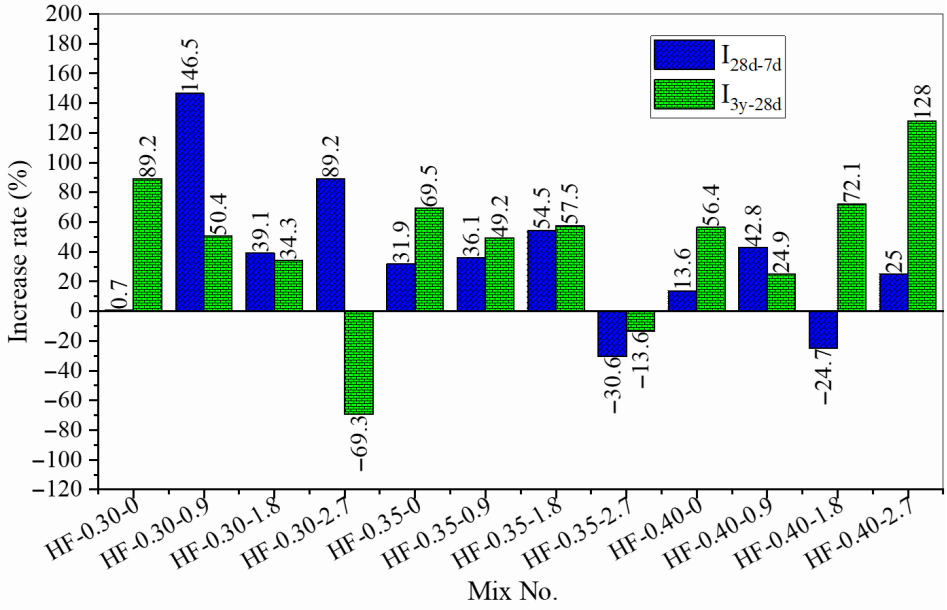


Figure 4. The increase ratio of compressive strength of HGPFRC at different curing ages.

4.2. Water Absorption Properties

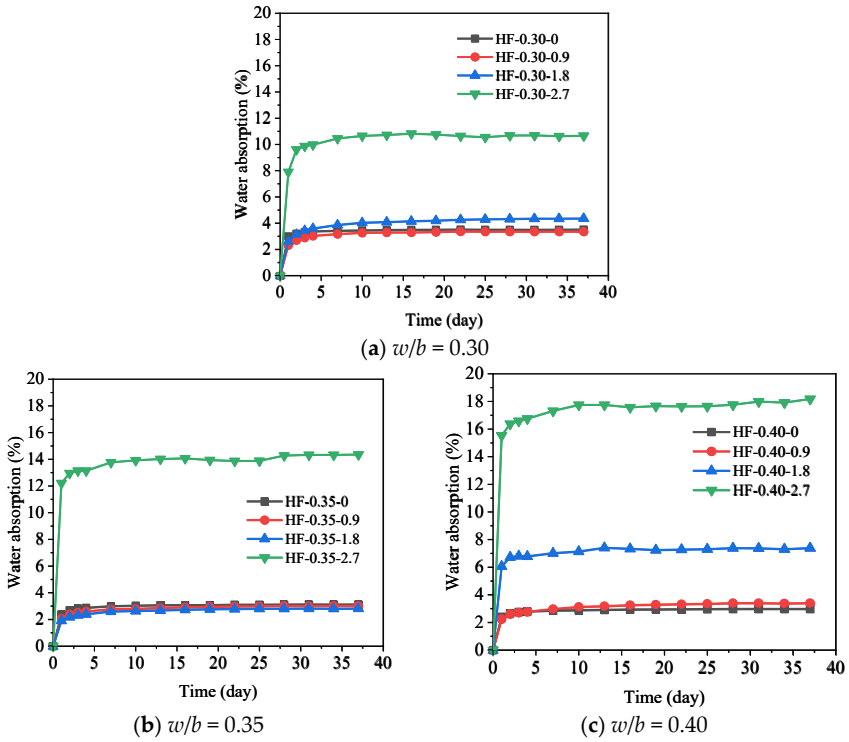
Table 4 shows the water absorption of HGPFRC at different testing periods, with values in parentheses representing standard deviations. Figure 5 depicts the full curves of water absorption of the specimens. It can be observed that the water absorption increased rapidly on the first day, followed by a relatively fast increase from day 1 to day 4 or day 7. Subsequently, the absorption curve tended to stabilize or rise slowly. In this study, the water absorption value at 31 days was selected as the evaluation index.

Table 4. The water absorption of the HGPFRC.

Mix ID	Water Absorption (%)							
	1 Day	2 Days	3 Days	4 Days	7 Days	28 Days	31 Days	37 Days
HF-0.30-0	2.99 (0.22)	3.19 (0.2)	3.3 (0.21)	3.37 (0.19)	3.42 (0.18)	3.5 (0.19)	3.49 (0.18)	3.51 (0.19)
HF-0.30-0.9	2.31 (0.15)	2.7 (0.19)	2.89 (0.18)	3.03 (0.11)	3.17 (0.11)	3.35 (0.02)	3.35 (0.02)	3.35 (0.02)
HF-0.30-1.8	2.59 (0.17)	3.13 (0.23)	3.43 (0.25)	3.59 (0.24)	3.86 (0.22)	4.31 (0.28)	4.34 (0.29)	4.35 (0.29)
HF-0.30-2.7	7.9 (0.56)	9.61 (0.3)	9.87 (0.67)	9.98 (0.93)	10.45 (1.09)	10.68 (1.81)	10.69 (1.65)	10.66 (1.68)
HF-0.35-0	2.37 (0.09)	2.69 (0.19)	2.82 (0.27)	2.87 (0.25)	2.99 (0.3)	3.11 (0.34)	3.12 (0.35)	3.12 (0.34)
HF-0.35-0.9	2.06 (0.2)	2.38 (0.21)	2.51 (0.26)	2.6 (0.22)	2.76 (0.25)	3.01 (0.32)	3 (0.31)	3.01 (0.31)
HF-0.35-1.8	1.91 (0.11)	2.18 (0.23)	2.32 (0.19)	2.39 (0.16)	2.59 (0.18)	2.8 (0.26)	2.81 (0.23)	2.81 (0.23)
HF-0.35-2.7	12.21 (1.12)	12.96 (0.88)	13.14 (0.93)	13.14 (0.93)	13.77 (0.89)	14.28 (0.82)	14.33 (0.66)	14.35 (0.71)
HF-0.40-0	2.4 (0.16)	2.65 (0.19)	2.75 (0.19)	2.79 (0.22)	2.85 (0.21)	2.97 (0.2)	2.97 (0.21)	2.97 (0.21)
HF-0.40-0.9	2.24 (0.05)	2.61 (0.06)	2.71 (0.14)	2.77 (0.17)	2.96 (0.18)	3.39 (0.15)	3.39 (0.14)	3.39 (0.14)
HF-0.40-1.8	6.06 (0.27)	6.72 (0.16)	6.81 (0.14)	6.78 (0.01)	7.01 (0.05)	7.38 (0.08)	7.36 (0.02)	7.38 (0.02)
HF-0.40-2.7	15.53 (1.33)	16.37 (1.37)	16.58 (1.34)	16.75 (1.2)	17.31 (1.17)	17.76 (1.23)	17.99 (1.2)	18.18 (1.11)

As shown in Table 4 and Figure 5, when w/b = 0.30, only HF-0.30-0.9 exhibited improved water absorption compared to HF-0.30-0, decreasing from 3.49% to 3.35%—a 4% reduction. As the hybrid fiber content increased, the water absorption of the concrete also increased, with HF-0.30-2.7 reaching 10.69%. When w/b = 0.35, the water absorption first decreased and then sharply increased with increasing fiber dosage. HF-0.35-0.9 and HF-0.35-1.8 exhibited water absorption of 3% and 2.81%, respectively, representing reductions of 3.85% and 9.94% compared to HF-0.35-0. Conversely, the water absorption of HF-0.35-2.7

reached 14.33%, a 359.29% increase over the control group. When w/b = 0.40, all hybrid fibers increased water absorption; the HF-0.40-2.7 exhibited a water absorption of 17.99%, more than five times that of HF-0.40-0. Figure 5 further indicates that HF-0.40-2.7's water absorption continues to show a pronounced upward trend.



(**a**) w/b = 0.30

(**b**) w/b = 0.35

(**c**) w/b = 0.40

Figure 5. The full curves of the water absorption of the HGPFRC.

Figure 6 examines the variation in the water absorption of HGPFRC with different w/b and fiber contents at various testing stages. In this figure, $R_{1d\text{-}0d}$, $R_{4d\text{-}1d}$, and $R_{31d\text{-}4d}$ represent the percentages of water absorption relative to the total 31-day water absorption for the first day (initial stage), from day 2 to day 4 (middle stage), and from day 5 to day 31 (later stage), respectively. It can be observed from Figure 6 that the water absorption of HGPFRC during the first day accounted for 60% to 86% of the total 31-day absorption. From day 2 to day 4, the water absorption constituted 6% to 23%, and from day 5 to day 31, it constituted 3% to 18% of the total.

When w/b = 0.30, the $R_{1d\text{-}0d}$ value of HF-0.30-0 was 86%, meaning the water absorption on the first day of immersion reached 86% of the total water absorption. After fiber addition, the $R_{1d\text{-}0d}$ value of HGPFRC first decreased and then increased, with all values lower than HF-0.30-0. The HF-0.30-1.8 exhibited the lowest $R_{1d\text{-}0d}$ at 60%. The $R_{4d\text{-}1d}$ value of HF-0.30-0 was 11%. After fiber addition, the $R_{4d\text{-}1d}$ of the concrete first increased and then decreased, with all values exceeding that of HF-0.30-0. Among them, the HF-0.30-1.8 exhibited the highest $R_{4d\text{-}1d}$ at 23%. The variation trend of $R_{31d\text{-}4d}$ in HGPFRC was identical to that of $R_{4d\text{-}1d}$. The HF-0.30-1.8 exhibited the highest $R_{31d\text{-}4d}$ at 17%. Specifically, when w/b = 0.30, the initial water absorption of HGPFRC was slower, while its mid-term and late-term water absorption were higher than those of non-fiber-reinforced HF-0.30-0.

When w/b = 0.35, in the early stage, the $R_{1d\text{-}0d}$ values for HF-0.35-0.9 and HF-0.35-1.8 were 69% and 68%, respectively, still significantly lower than HF-0.35-0, but the decrease was not as pronounced as when w/b = 0.30. In the mid-term and late stages, both $R_{4d\text{-}1d}$ and $R_{31d\text{-}4d}$ for HF-0.35-0.9 and HF-0.35-1.8 exceeded those of HF-0.35-0.

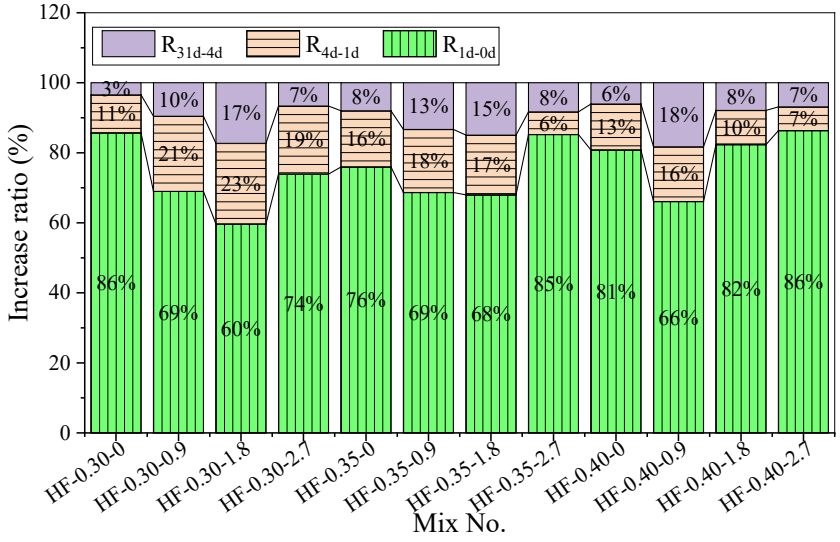


Figure 6. Proportion of water absorption at different time periods.

When w/b = 0.40, the early, mid, and late water absorption of HF-0.40-0 were 81%, 13% and 6%, respectively. After fiber addition, only HF-0.40-0.9 exhibited an $R_{1d\text{-}0d}$ lower than HF-0.40-0 at 66%. Its mid-stage and late-stage water absorption were 16% and 18%, respectively, exceeding those of HF-0.40-0.

The above analysis indicated that the w/b and the dosage of hybrid fibers significantly influence the water absorption properties of HGPFRC at different stages.

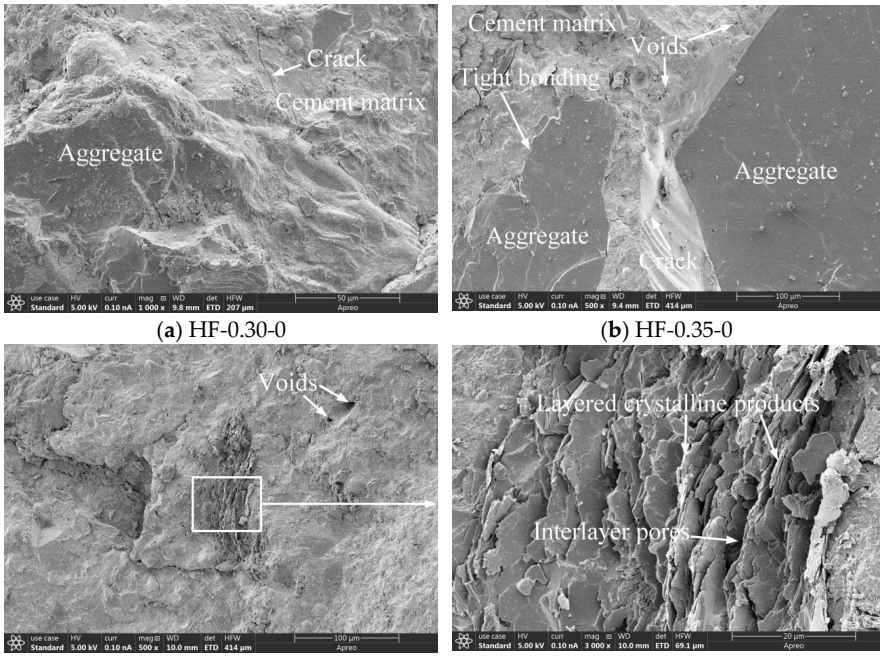
Based on the capillary absorption theory proposed by Hall [58,59], the water absorption process of concrete was driven by capillary action, and its sorptivity served as a critical parameter for characterizing the pore structure of the material. This theory delineated the absorption process into distinct stages, corresponding to the filling of pores of different size scales. In the present study, the initial stage ($R_{1d\text{-}0d}$) primarily reflected the filling rate of open surface pores and large capillary pores; the intermediate stage ($R_{4d\text{-}1d}$) corresponded to the slower absorption by smaller capillary pores; and the later stage ($R_{31d\text{-}4d}$) involved the long-term permeation behavior of micropores and the interfacial transition zone (ITZ). This analytical approach was highly consistent with the core principles of capillary absorption theory.

Recent investigations into the water absorption behavior of FRC provided important references for the interpretation of the current results. Nan F et al. [60], in their study on steel fiber-reinforced concrete, found that fibers influence moisture transport through two primary mechanisms: the interaction at the fiber–matrix interface and the physical blocking effect of the fibers. In this study, the continued increase in the later-stage absorption rate of the HF-0.40-2.7 specimens could be attributed to microcracks introduced at the interface due to the excessively high fiber content, which act as pathways for long-term moisture ingress. Drawing on the findings of studies regarding the influence of fibers on pore structure [60,61], an in-depth discussion on the relationship between fiber dosage and permeation pathways was provided: at a low fiber content (0.9%), fibers were dispersed uniformly, refining the pore structure, increasing pore tortuosity, and reducing permeability; at the optimal fiber content (1.8%), fibers formed a moderate spatial network within the cementitious matrix, optimizing the ITZ and resulting in the most compact pore structure; and at a high fiber content (2.7%), the risk of fiber agglomeration increased, leading to greater matrix porosity and consequently higher water absorption at later stages. CT scanning studies on basalt fiber-reinforced concrete by Zhao et al. [62] confirmed that the effect of fiber content on porosity was non-linear, with an optimal content maximizing the proportion of harmless pores. Valizadeh Kiamahalleh et al. [61] also found that exceeding

the optimal fiber content led to fiber agglomeration, which increased pore connectivity and degraded performance. These quantitative findings were in strong agreement with the evolution of the water absorption rate observed in the present study. Furthermore, the water absorption behavior observed at a fiber content of 2.7% also helped explain the reduction in strength; the substantial increase in internal porosity resulted in a poorly compacted internal structure of the concrete specimens, leading to a significant decrease in compressive strength.

4.3. Microstructure

The SEM image analysis in this study was primarily qualitative, aimed at identifying the fiber—matrix interfacial condition, the morphology of cracks on the cementitious matrix surface, and the surface characteristics of the fibers. Figure 7 shows SEM images of HF-0.30-0 and HF-0.35-0. The cement matrix surface primarily exhibited a structurally dense C-S-H gel product, with very tight bonding between the cement matrix and aggregates. However, noticeable cracks were present on the matrix surface, and some pores were also visible on the cement matrix in Figure 7b. In Figure 7c, layered crystalline products were intercalated among the gel products, with distinct interlayer voids visible between these crystalline layers (Figure 7d).



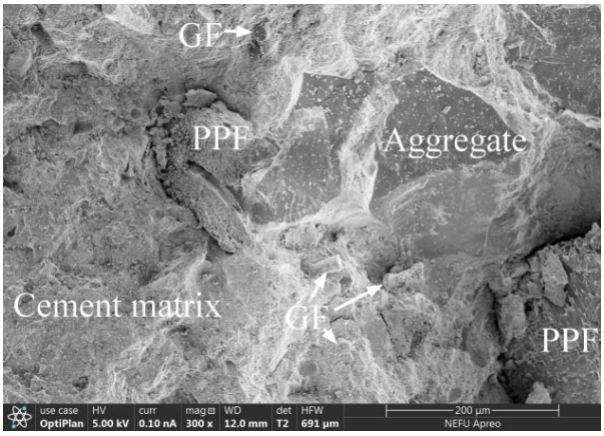
(**a**) HF-0.30-0 (**b**) HF-0.35-0

(**c**) HF-0.35-0 (**d**) HF-0.35-0

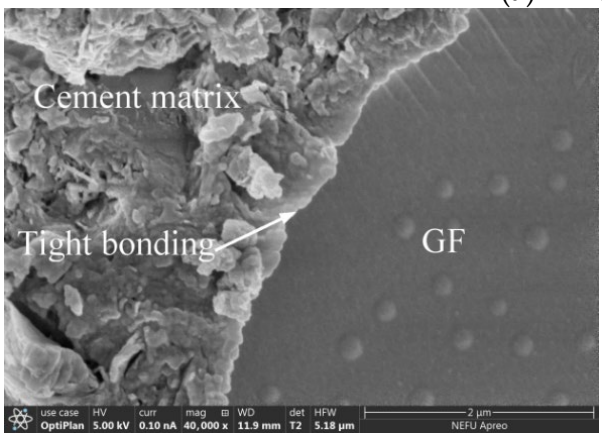
Figure 7. SEM images of HF-0.30-0 and HF-0.35-0.

Figure 8 shows the SEM images of HF-0.35-1.8. The GF and PPF were uniformly distributed within the concrete matrix, forming an interwoven network. Both GF and PPF exhibited excellent bonding with the cementitious matrix, particularly the GF, which appear tightly bonded under 40,000× magnification. The cementitious matrix exhibited minimal pores and cracks, forming a dense structure. This likely represented the primary reason for HF-0.35-1.8's optimal compressive strength and the lowest water absorption. Hu Jiyuan et al. [63] employed SEM to observe the ITZ of hybrid fiber-reinforced recycled concrete and found that when the fiber content was moderate, the fiber–matrix interface exhibited good bonding, with hydration products adequately covering the fiber surface. This observation was consistent with the findings for the HF-0.35-1.8 group in the present study. Nováková et al. [64] conducted SEM analysis on the ITZ of basalt fiber-reinforced concrete and

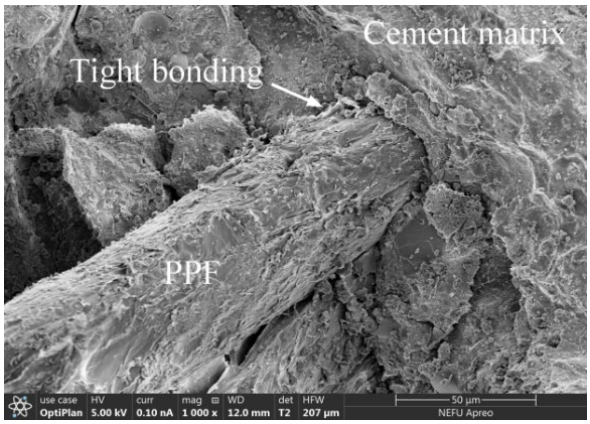
noted that the compactness of the fiber–matrix interface was positively correlated with macroscopic mechanical properties, and a good interfacial bond could effectively enhance its strength characteristics. This finding aligned well with the relatively high 3-year strength observed in the HF-0.35-1.8 group of this study.



(**a**) HF-0.35-1.8



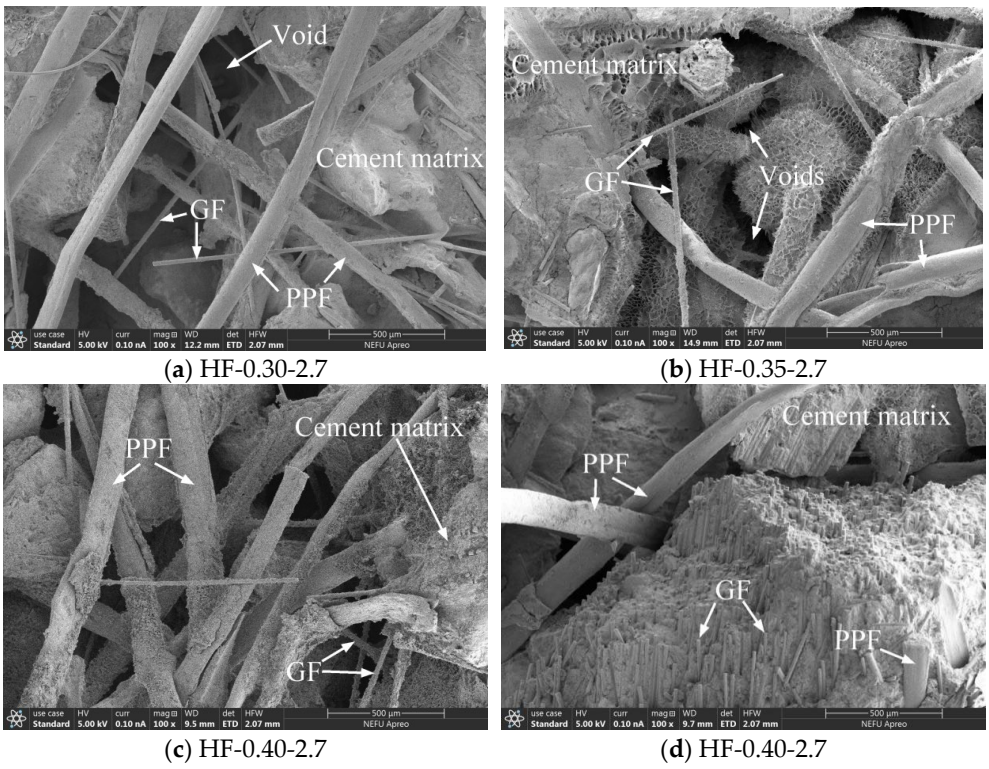
(**b**) HF-0.35-1.8



(**c**) HF-0.35-1.8

Figure 8. SEM images of HF-0.35-1.8.

Figure 9 shows the SEM images of concrete with a hybrid fiber content of 2.7%. It revealed numerous fibers within the concrete matrix, enveloped by only a minimal amount of cementitious matrix. The voids between different fibers remained unfilled or incompletely filled by the cementitious matrix. In HF-0.40-2.7, fiber "agglomeration" was also observed. These phenomena were all caused by excessive fiber content. Macroscopically, this manifested as extremely low compressive strength and high water absorption. As shown in Figure 3, across all w/b and curing ages, compressive strength sharply declined when the hybrid fiber content reached 2.7%, indicating a negative hybrid effect of fibers. The negative hybrid effect in FRC arose inevitably from the small monofilament diameter of flexible fibers and the minimal spacing between fibers within the matrix once a certain threshold was reached. Beyond a certain fiber dosage, fibers overlapped and interfered with each other, reducing the contact surface area between fibers and the matrix and diminishing the number of fibers contributing to reinforcement [35]. At this fiber dosage, when concrete specimens failed under compressive loading, virtually no coarse aggregate fragmentation occurred internally, and fiber breakage was also minimal. The failure was almost entirely attributed to the dispersion of fibers enveloped by the cementitious matrix. At this point, the concrete had already lost its value for engineering applications.



(**a**) HF-0.30-2.7 (**b**) HF-0.35-2.7

(**c**) HF-0.40-2.7 (**d**) HF-0.40-2.7

Figure 9. SEM images of the specimens containing 2.7% hybrid fibers.

5. Conclusions

This article systematically studied the development of mechanical properties, water absorption performance, and microstructure of HGPFRC, and drew the following main conclusions.

1. The w/b and hybrid fiber content significantly influence the compressive strength development rate of HGPFRC. From days 7 to 28 of curing, the compressive strength gain rate of HGPFRC exceeded that of the fiber-free control group. However, during the initial 7 days and from day 28 to 3 years, the compressive strength gain rate of HGPFRC was lower than that of the control group.
2. HGPFRC with varying w/b and fiber contents exhibited significant differences in water absorption across different testing stages. The HGPFRC achieved 60% to 86% of total water absorption within the first day, with 6% to 23% occurring between days 2 and 4, and 3% to 18% between days 5 and 31. These findings provide valuable reference for selecting testing time points in concrete water absorption experiments.
3. Considering strength, water absorption, and microstructure comprehensively, the HF-0.35-1.8 group—with a w/b of 0.35 and a hybrid fiber content of 1.8%—emerged as the optimal mix design in this study. Its 28-day and 3-year compressive strengths reached 37.4 MPa and 58.9 MPa, respectively, representing increases of 23.84% and 15.04% compared to the control group. Its water absorption on day 1 and day 31 were only 1.91% and 2.81%, respectively, showing reductions of 19.41% and 9.94% compared to the fiber-free control group.
4. In this study, the 2.7% volume fraction of hybrid GF and PPF significantly exceeded the optimal dosage. At this point, the concrete's compressive strength rapidly decreased, and water absorption increased markedly. SEM analysis revealed a loose internal structure, indicating that the concrete could no longer meet construction requirements.

Author Contributions: Conceptualization, L.Y. and Z.Y.; Methodology, L.Y. and Z.Y.; Software, L.Y. and Z.Y.; Validation, Z.Y.; Formal analysis, L.Y. and Z.Y.; Investigation, Z.Y.; Resources, Z.Y.; Data curation, L.Y. and Z.Y.; Writing—original draft, Z.Y.; Writing—review & editing, Z.Y.; Visualization, L.Y. and Z.Y.; Supervision, Z.Y.; Project administration, Z.Y.; Funding acquisition, L.Y. and Z.Y. All authors have read and agreed to the published version of the manuscript.

Funding: This research was funded by Heilongjiang University grant number 2023-KYYWF-1443.

Data Availability Statement: The original contributions presented in this study are included in the article. Further inquiries can be directed to the corresponding author.

Acknowledgments: This work was supported by the Basic Research Project of Scientific Research Funds for Provincial Universities of Heilongjiang Province, and the Basic Scientific Research Business Expenses of Provincial Universities and Colleges in Heilongjiang Province (2023-KYYWF-1443).

Conflicts of Interest: The authors declare no conflicts of interest.

References

1. Kizilkanat, A.B.; Kabay, N.; Akyüncü, V.; Chowdhury, S.; Akça, A.H. Mechanical properties and fracture behavior of basalt and glass fiber reinforced concrete: An experimental study. *Constr. Build. Mater.* **2015**, *100*, 218–224. [CrossRef]
2. Pakravan, H.R.; Ozbakkaloglu, T. Synthetic fibers for cementitious composites: A critical and in-depth review of recent advances. *Constr. Build. Mater.* **2019**, *207*, 491–518. [CrossRef]
3. Yin, S.; Tuladhar, R.; Shi, F.; Combe, M.; Collister, T.; Sivakugan, N. Use of macro plastic fibres in concrete: A review. *Constr. Build. Mater.* **2015**, *93*, 180–188. [CrossRef]
4. Tassew, S.T.; Lubell, A.S. Mechanical properties of glass fiber reinforced ceramic concrete. *Constr. Build. Mater.* **2014**, *51*, 215–224. [CrossRef]
5. Mehta, P.K.; Monteiro, P.J.M. *Concrete: Microstructure, Properties and Materials*, 4th ed.; McGraw-Hill Professional: Columbus, OH, USA, 2014.
6. Wang, X.; Li, L.; Wei, M.; Xiang, Y.; Wu, Y.; Zhou, B.; Sun, Y.; Cheng, W. Experimental study on the mechanical properties of short-cut basalt fiber reinforced concrete under large eccentric compression. *Sci. Rep.* **2025**, *15*, 10845. [CrossRef]
7. Tagnit-Hamou, A.; Vanhove, Y.; Petrov, N. Microstructural analysis of the bond mechanism between polyolefin fibers and cement pastes. *Cem. Concr. Res.* **2005**, *35*, 364–370. [CrossRef]
8. Zhen, H.; Xiong, Z.; Song, Y.; Li, L.; Qiu, Y.; Zou, X.; Chen, B.; Chen, D.; Liu, F.; Ji, Y. Early mechanical performance of glass fibre-reinforced manufactured sand concrete. *J. Build. Eng.* **2024**, *83*, 108440. [CrossRef]
9. Enfedaque, A.; Cendón, D.; Gálvez, F.; Sánchez-Gálvez, V. Analysis of glass fiber reinforced cement (GRC) fracture surfaces. *Constr. Build. Mater.* **2010**, *24*, 1302–1308. [CrossRef]
10. Gao, Y.; Cheng, Z.; Yu, J.; Guo, X.; Liu, Y.; Chen, W. Mechanical performance enhancement of UHPC via ITZ improvement using graphene oxide-coated steel fibers. *Cem. Concr. Compos.* **2025**, *157*, 105931. [CrossRef]
11. Du, Y.; Lu, S.; Wang, Z.; Bai, Q.; Huang, H.; Xu, J. Research on evolutionary patterns of dynamic mechanical and energy characteristics in carbon fiber-reinforced concrete and intelligent predictive modeling. *J. Build. Eng.* **2026**, *117*, 114855. [CrossRef]
12. Zhou, M.; He, X.; Wang, H.; Wei, B.; Tang, Z. Fatigue bond behavior between basalt fiber reinforced polymer bars and steel fiber reinforced concrete. *Compos. Struct.* **2026**, *377*, 119812. [CrossRef]
13. Wu, T.; Yang, X.; Wei, H.; Liu, X. Mechanical properties and microstructure of lightweight aggregate concrete with and without fibers. *Constr. Build. Mater.* **2019**, *199*, 526–539. [CrossRef]
14. Juarez, C.; Fajardo, G.; Monroy, S.; Duran-Herrera, A.; Valdez, P.; Magniont, C. Comparative study between natural and PVA fibers to reduce plastic shrinkage cracking in cement-based composite. *Constr. Build. Mater.* **2015**, *91*, 164–170. [CrossRef]
15. Sadrmomtazi, A.; Tahmouresi, B.; Saradar, A. Effects of silica fume on mechanical strength and microstructure of basalt fiber reinforced cementitious composites (BFRCC). *Constr. Build. Mater.* **2018**, *162*, 321–333. [CrossRef]
16. Jiang, C.; Fan, K.; Wu, F.; Chen, D. Experimental study on the mechanical properties and microstructure of chopped basalt fibre reinforced concrete. *Mater. Des.* **2014**, *58*, 187–193. [CrossRef]
17. Savastano, H.; Santos, S.; Radonjic, M.; Soboyejo, W. Fracture and fatigue of natural fiber-reinforced cementitious composites. *Cem. Concr. Compos.* **2009**, *31*, 232–243. [CrossRef]
18. Yehia, S.; Douba, A.; Abdullahi, O.; Farrag, S. Mechanical and durability evaluation of fiber-reinforced self-compacting concrete. *Constr. Build. Mater.* **2016**, *121*, 120–133. [CrossRef]
19. Pająk, M.; Ponikiewski, T. Flexural behavior of self-compacting concrete reinforced with different types of steel fibers. *Constr. Build. Mater.* **2013**, *47*, 397–408. [CrossRef]

20. Koohestani, B.; Darban, A.K.; Mokhtari, P.; Yilmaz, E.; Darezereshki, E. Comparison of different natural fiber treatments: A literature review. *Int. J. Environ. Sci. Technol.* **2019**, *16*, 629–642. [CrossRef]
21. Zhang, P.; Li, Q.-F. Effect of polypropylene fiber on durability of concrete composite containing fly ash and silica fume. *Compos. Part B* **2013**, *45*, 1587–1594. [CrossRef]
22. Babafemi, A.J.; Boshoff, W.P. Tensile creep of macro-synthetic fibre reinforced concrete (MSFRC) under uni-axial tensile loading. *Cem. Concr. Compos.* **2015**, *55*, 62–69. [CrossRef]
23. Tang, J.P.; Feng, R.; Quach, W.M.; Zeng, J.J. Axial compressive behaviour of simulated corrosion-damaged RC columns retrofitted with UHPFRC jackets subjected to dry-wet cycling condition. *Constr. Build. Mater.* **2024**, *424*, 135956. [CrossRef]
24. Tang, J.P.; Feng, R.; Quach, W.M.; Zeng, J.J. Evaluation of flexural performance on corrosion-damaged RC beams retrofitted with UHPFRCC under marine exposure. *Eng. Struct.* **2025**, *333*, 120193. [CrossRef]
25. Pehlivanlı, Z.O.; Uzun, I.; Demir, I. Mechanical and microstructural features of autoclaved aerated concrete reinforced with autoclaved polypropylene, carbon, basalt and glass fiber. *Constr. Build. Mater.* **2015**, *96*, 428–433. [CrossRef]
26. Simões, T.; Costa, H.; Dias-Da-Costa, D.; Júlio, E. Influence of fibres on the mechanical behaviour of fibre reinforced concrete matrixes. *Constr. Build. Mater.* **2017**, *137*, 548–556. [CrossRef]
27. Choi, Y.; Yuan, R.L. Experimental relationship between splitting tensile strength and compressive strength of GFRC and PFRC. *Cem. Concr. Res.* **2005**, *35*, 1587–1591. [CrossRef]
28. Beigi, M.H.; Berenjian, J.; Omran, O.L.; Nik, A.S.; Nikbin, I.M. An experimental survey on combined effects of fibers and nanosilica on the mechanical, rheological, and durability properties of self-compacting concrete. *Mater. Des.* **2013**, *50*, 1019–1029. [CrossRef]
29. Sivakumar, A.; Santhanam, M. Mechanical properties of high strength concrete reinforced with metallic and non-metallic fibres. *Cem. Concr. Compos.* **2007**, *29*, 603–608. [CrossRef]
30. Barluenga, G.; Hernández-Olivares, F. Cracking control of concretes modified with short AR-glass fibers at early age. Experimental results on standard concrete and SCC. *Cem. Concr. Res.* **2007**, *37*, 1624–1638. [CrossRef]
31. Ali, B.; Raza, S.S.; Hussain, I.; Iqbal, M. Influence of different fibers on mechanical and durability performance of concrete with silica fume. *Struct. Concr.* **2020**, *21*, 318–333. [CrossRef]
32. Xue, G.; Yilmaz, E.; Song, W.; Yilmaz, E. Influence of fiber reinforcement on mechanical behavior and microstructural properties of cemented tailings backfill. *Constr. Build. Mater.* **2019**, *213*, 275–285. [CrossRef]
33. Xue, G.; Yilmaz, E.; Song, W.; Cao, S. Mechanical, flexural and microstructural properties of cement-tailings matrix composites: Effects of fiber type and dosage. *Compos. Part B* **2019**, *172*, 131–142. [CrossRef]
34. Behfarnia, K.; Behravan, A. Application of high performance polypropylene fibers in concrete lining of water tunnels. *Mater. Des.* **2014**, *55*, 274–279. [CrossRef]
35. Afroughsabet, V.; Ozbakkaloglu, T. Mechanical and durability properties of high-strength concrete containing steel and polypropylene fibers. *Constr. Build. Mater.* **2015**, *94*, 73–82. [CrossRef]
36. Li, J.J.; Niu, J.G.; Wan, C.J.; Jin, B.; Yin, Y.L. Investigation on mechanical properties and microstructure of high performance polypropylene fiber reinforced lightweight aggregate concrete. *Constr. Build. Mater.* **2016**, *118*, 27–35. [CrossRef]
37. Fallah, S.; Nematzadeh, M. Mechanical properties and durability of high-strength concrete containing macro-polymeric and polypropylene fibers with nano-silica and silica fume. *Constr. Build. Mater.* **2017**, *132*, 170–187. [CrossRef]
38. Abaeian, R.; Behbahani, H.P.; Moslem, S.J. Effects of high temperatures on mechanical behavior of high strength concrete reinforced with high performance synthetic macro polypropylene (HPP) fibres. *Constr. Build. Mater.* **2018**, *165*, 631–638. [CrossRef]
39. Hua, Y.; Lian, J.; Zhou, T. Effect of Aspect Ratio on Mechanical Properties of Hybrid Fiber-Reinforced Concrete. *J. Build. Mater.* **2005**, *8*, 71–76. (In Chinese) [CrossRef]
40. Pakravan, H.; Latifi, M.; Jamshidi, M. Hybrid short Fiber Reinforcement System in Concrete: A Review. *Constr. Build. Mater.* **2017**, *142*, 280–294. [CrossRef]
41. Liu, J.; Jia, Y.; Wang, J. Experimental Study on Mechanical and Durability Properties of Glass and Polypropylene Fiber Reinforced Concrete. *Fibers Polym.* **2019**, *20*, 1900–1908. [CrossRef]
42. de Melo, F.M.C.; de Jesus Cruz, A.C.A.; de Souza Netto, L.D.; de Souza Simplício, M.A. Experimental study of bond between steel bars and hybrid fibers reinforced concrete. *Constr. Build. Mater.* **2021**, *275*, 122176. [CrossRef]
43. Hou, L.; Zhang, X.; Huang, W.; Zhang, X. Uniaxial Compression Behavior of Polypropylene and Glass Fiber-Reinforced Desert Sand Concrete. *Arab. J. Sci. Eng.* **2024**, *50*, 16679–16696. [CrossRef]
44. Islam, S.U.; Waseem, S.A. An experimental study on mechanical and fracture characteristics of hybrid fibre reinforced concrete. *Structures* **2024**, *68*, 107053. [CrossRef]
45. Hou, L.; Wen, B.; Huang, W.; Zhang, X.; Zhang, X. Mechanical Properties and Microstructure of Polypropylene–Glass-Fiber-Reinforced Desert Sand Concrete. *Polymers* **2023**, *15*, 4675. [CrossRef]
46. Hou, L.; Jian, S.; Huang, W. The Effect of Polypropylene Fiber and Glass Fiber on the Frost Resistance of Desert Sand Concrete. *KSCE J. Civ. Eng.* **2023**, *28*, 342–353. [CrossRef]

47. Vadivel, M.; Selinaruby, G.; Padmapriya, R.; Perumal, B. Experimental research on mechanical and microstructural characteristics of hybrid fiber reinforced concrete (HFRC). *Sci. Rep.* **2025**, *15*, 43189. [CrossRef]
48. Dharek, M.S.; M, M.; S, B.; Vengala, J.; Tangadagi, R.B. Performance evaluation of hybrid fiber reinforced concrete on engineering properties and life cycle assessment: A sustainable approach. *J. Clean. Prod.* **2024**, *458*, 142498. [CrossRef]
49. *JGJ 55-2011*; Specification for Mix Proportion Design of Ordinary Concrete. CS (Chinese Standard): Beijing, China, 2011. (In Chinese)
50. Bankir, M.B.; Sevim, U.K. Performance optimization of hybrid fiber concrete according to mechanical properties. *Constr. Build. Mater.* **2020**, *261*, 119952. [CrossRef]
51. *CECS 13-2009*; Standard Test Methods for Fiber Reinforced Concrete. CS (Chinese Standard): Beijing, China, 2009. (In Chinese)
52. *GB/T 50081-2019*; Standard for Test Method of Mechanical Properties on Ordinary Concrete. CS (Chinese Standard): Beijing, China, 2019. (In Chinese)
53. *ASTM C642*; Standard Test Method for Density, Absorption, and Voids in Hardened Concrete, Annual Book of ASTM Standard. ASTM International: West Conshohocken, PA, USA, 2013.
54. *ASTM C1723*; Standard Guide for Examination of Hardened Concrete Using Scanning Electron Microscopy, Annual Book of ASTM Standard. ASTM International: West Conshohocken, PA, USA, 2010.
55. Marom, G.; Fischer, S.; Tuler, F.R.; Wagner, H.D. Hybrid effects in composites: Conditions for positive or negative effects versus rule-of-mixtures behaviour. *J. Mater. Sci.* **1978**, *13*, 1419–1426. [CrossRef]
56. Fu, S.Y.; Mai, Y.W.; Lauke, B.; Yue, C.Y. Synergistic effect on the fracture toughness of hybrid short glass fiber and short carbon fiber reinforced polypropylene composites. *Mater. Sci. Eng. A* **2002**, *323*, 326–335. [CrossRef]
57. Bentur, A.; Mindess, S. *Fibre Reinforced Cementitious Composites*, 2nd ed.; Taylor & Francis: London, UK, 2007.
58. Hall, C. Water sorptivity of mortars and concrete—A review. *Mag. Concr. Res.* **1993**, *419*, 51–61. [CrossRef]
59. Hall, C.; Yau, M.H.R. Water movement in porous building materials—IX. The water absorption and sorptivity of concretes. *Build. Environ.* **1987**, *22*, 77–82. [CrossRef]
60. Nan, F.; Shen, Q.; Zou, S.; Yang, H.; Sun, Z.; Yang, J. Capillary Water Absorption Characteristics of Steel Fiber-Reinforced Concrete. *Buildings* **2025**, *15*, 1542. [CrossRef]
61. Kiamahalleh, M.V.; Gholampour, A.; Shahmirzadi, M.R.; Ngo, T.D.; Ozbakkaloglu, T. Mechanical, Durability, and Microstructure Assessment of Wastepaper Fiber-Reinforced Concrete Containing Metakaolin. *Materials* **2024**, *17*, 2608. [CrossRef]
62. Zhao, J.; Wang, X.; Yan, F.; Cai, X.; Xiao, S.; Cui, S.; Liu, P. Investigation of the Evolutionary Patterns of Pore Structures and Mechanical Properties During the Hydration Process of Basalt-Fiber-Reinforced Concrete. *Materials* **2025**, *18*, 3212. [CrossRef]
63. Hu, J.; Sheng, D.; Qin, F.; Huo, X.; Chai, Z. Study on Mechanical Properties of Hybrid Fiber-Reinforced Recycled Coarse Aggregate Concrete Based on DIC Method. *Bull. Silic. Res.* **2024**, *43*, 3745–3754. (In Chinese)
64. Nováková, I.; Jhatial, A.A.; Kekez, S.; Gjerløw, E.; Gulik, V.; Kannathasan, K.R.; Vaišnoras, M.; Krasnikovs, A. Investigating the Influence of Oil Shale Ash and Basalt Composite Fibres on the Interfacial Transition Zone in Concrete. *Buildings* **2024**, *14*, 1952. [CrossRef]

Disclaimer/Publisher's Note: The statements, opinions and data contained in all publications are solely those of the individual author(s) and contributor(s) and not of MDPI and/or the editor(s). MDPI and/or the editor(s) disclaim responsibility for any injury to people or property resulting from any ideas, methods, instructions or products referred to in the content.